

Article

Predefined-Time and Prescribed-Performance Control Methods Combined with Second-Order Terminal Sliding Mode Control for an Unmanned Planing Hull System with Input Delay and Unknown Disturbance

Seongik Han 

Department of Mechanical System Engineering, Dongguk University WISE Campus,
Gyeongju 38066, Republic of Korea; skhan@dongguk.ac.kr; Tel.: +82-54-770-2222

Abstract: In this study, we investigate a terminal sliding mode control (TSMC) system combined with predefined-time and prescribed-performance control methods for an unmanned planing hull (UPH) system in the presence of a control input delay at the heading axis and a porpoising motion due to pitching-moment disturbance. A second-order TSMC system is adopted to bypass the unstable heading-angle response of the conventional first-order TSMC system caused by the control input delay of the hydraulic rudder actuator system. Next, predefined-time and prescribed-performance control methods are proposed to enhance the disturbance rejection performance of an uncertain UPH. The results of sequential comparative simulations show that the disturbance rejection performance of the proposed hybrid disturbance rejector using both the predefined-time and prescribed-performance control methods for a porpoising motion is superior to those of conventional controller systems without introducing disturbance observers.

Keywords: unmanned planing hull system; control input delay; second-order terminal sliding mode control; predefined-time control; prescribed-performance control



Citation: Han, S. Predefined-Time and Prescribed-Performance Control Methods Combined with Second-Order Terminal Sliding Mode Control for an Unmanned Planing Hull System with Input Delay and Unknown Disturbance. *J. Mar. Sci. Eng.* **2023**, *11*, 2191. <https://doi.org/10.3390/jmse11112191>

Academic Editor: Rafael Morales

Received: 28 October 2023

Revised: 13 November 2023

Accepted: 16 November 2023

Published: 17 November 2023



Copyright: © 2023 by the author. Licensee MDPI, Basel, Switzerland. This article is an open access article distributed under the terms and conditions of the Creative Commons Attribution (CC BY) license (<https://creativecommons.org/licenses/by/4.0/>).

1. Introduction

Unmanned surface vehicles (USVs) are marine crafts that can conduct unmanned missions for operations in dangerous areas, harsh environments, polluted areas, or nuclear-contaminated sites. They can be operated remotely or automatically by pilots from safe locations with minimal human intervention. USVs are investigated increasingly in marine engineering areas related to marine robotic vehicles, which provide guidance, navigation, and control for intelligence, coastal surveillance, reconnaissance, scientific marine research studies, and commercial and military purposes.

Among the many types of USVs, a planing hull (PH) [1] is a sea surface vehicle in which the weight of the vehicle is supported by the generated hydraulic pressure in the vehicle during high-speed navigation. This pressure provides a lift force, which decreases the vehicle surface resistance. The PH demonstrates high boarding sensitivity in calm-sea-surface environments; however, under high waves, its boarding sensitivity deteriorates and adversely affects the vehicle body. This problem can be partially avoided by constructing a V-shaped PH. However, the size of the hull is limited because the PH requires high engine power. Nonetheless, PHs are widely used in various fields, such as high-speed patrol vessels, racing, and leisure vessels. The weight of a PH in the low-speed range is supported only by buoyancy forces such as the displacement of ships.

Unmanned PH (UPH) control technologies for automatic navigation include speed and steering control systems. Propeller thrust is typically used in surge speed control systems. The steering control system for the course-keeping control of a UPH includes a hydraulic motor pump, hydraulic cylinder, servo motor, and rudder. The control configuration of

the surface vessel is disadvantageous as it allows only two actuators to be used for motion with three degrees-of-freedom (DOFs). The propeller thrust is applied to control the surge speed and, thus, both the sway displacement and heading are controlled by only the rudder action. Moreover, directly compensating for the unmatched disturbance of the porpoising motion in the pitching axis using only two actuators is challenging. Thus, the rudder control action must be improved to simultaneously compensate for both the deviation from the guided path and porpoising motion disturbances caused by the pitching moment transferred from the pitch axis, as well as to enhance surge control.

Sliding mode control (SMC) [2] is a widely used control method that is theoretically simple and robust against external uncertainties. Thus, SMC has been applied to the course-tracking system of USVs [3–6]. However, the switching operation involved results in negative chattering [7]. To overcome this issue, the boundary layer theory was established. Nonetheless, performance degradation remains. As an alternative to conventional SMC, terminal sliding mode control (TSMC) [8–10] was investigated to realize faster tracking and better disturbance rejection with only mild chattering. TSMC was applied for path following and course keeping in USVs [11–16]. However, the finite convergence time of a TSMC system is typically an unbounded function with respect to the initial conditions of the system and is conservative in most cases. Moreover, obtaining a direct relationship between a fixed stabilization time and the tuning control parameters is challenging.

When UPHs are underactuated, unmatched disturbances typically exist, in which uncertain external disturbances are not directly coupled to the control input. In particular, direct compensation for the pitching moment generated along the pitch axis is challenging if the hull form is not designed appropriately to prevent the pitching-moment effect. Meanwhile, an additional trim tab and interceptor [17–19] were introduced to regulate the pitching moment. Meanwhile, the hull form is designed to reduce the pitching moment. The control input boat trim, and a maneuvering posture was adopted to address the low wave resistance. Consequently, the surge speed increased and fuel consumption decreased. However, equipping these additional devices on boats increases the cost of designing and manufacturing the UPH, as well as increasing system complexity. Moreover, conventional disturbance observers [20–22] and extended state observers [23–26] have been used to estimate the external disturbance in USV systems. Most of these observers are applied based on matched uncertainty. Moreover, adopting a disturbance observer increases the control system complexity and computing time.

Inspired by the aforementioned finding, first, the concept of predefined-time control was developed [27–29] to achieve fast responses and improve robustness to uncertainty. The distinguishing advantage of predefined-time control is that the system settling time is determined explicitly by the tuning parameters and can be defined in advance. Moreover, a partial improvement in uncertainty was achieved. Predefined-time control has recently been employed for the attitude control of rigid spacecraft systems [30–32], multi-agent systems [33–36], and USV systems [37,38]. However, predefined-time control prefers to achieve time-domain performance via direct parameter choice. Thus, the disturbance rejection effect by only utilizing this scheme is likely to be weak. Applications for the disturbance rejection of a predefined-time control scheme have been rather scarce, until now.

However, as another constraint control method, prescribed-performance controls [38–42] are considered to obtain greater robustness to unmatched pitching-moment disturbances without requiring a complex disturbance observer in this study. Prescribed-performance control implies that the tracking error should converge to an arbitrarily prescribed small steady state bound with an appropriate convergence rate and exhibit a maximum overshoot of less than a sufficiently small predefined value. Based on the prescribed performance, the steady state and transient performances against uncertainty were improved by applying a USV system [43–47]. However, the conventional prescribed-performance control adopted the complex variable transformation that results in a complicated controller structure. In this study, based on the idea that the robustness of the control system with the prescribed-performance control can partially exert a disturbance depression, the prescribed-

performance control applied in [42] was adopted without explicit dependence on the disturbance observer. The adopted prescribed-performance control term requires a simpler variable transformation than that presented in [36–41]. Notably, the predefined control performance can be achieved by adding the prescribed control term.

In this study, a disturbance rejector utilizing both predefined-time and prescribed-performance control methods is introduced to maximize the disturbance rejection performance against an unmatched pitching moment exerting an effect on the heading axis.

The main contributions of this study are as follows:

- (1) Porpoising disturbance due to the pitching moment of UPH systems was assumed to enhance sensitivity to variations in the unmatched uncertainties of UPH systems.
- (2) A second-order TSMC system was designed to accommodate the control input delay in a hydraulic rudder actuator system.
- (3) A second-order TSMC system with predefined-time control was designed to achieve improved settling-time convergence and robustness to unmatched disturbances when compared with a conventional TSMC system. Furthermore, it aimed to achieve a faster and more stable heading-angle response by the UPH than conventional TSMC for a perturbed environment.
- (4) Predefined-time and prescribed-performance control methods were used simultaneously for the first time to maximize the rejection performance and obtain stable tracking performance for an unmatched pitching-moment disturbance without adopting a complex disturbance observer. Consequently, the tracking performance of the heading-angle axis was largely improved by utilizing the proposed hybrid disturbance rejector.
- (5) The proposed second-order TSMC system with a hybrid disturbance rejector facilitated by predefined-time and prescribed-performance control exhibited a simpler controller structure than the conventional robust control systems equipped with a complex disturbance observer to estimate the disturbance.
- (6) To the best of our knowledge, predefined-time and prescribed-performance control methods have not been applied simultaneously in the field of USV control to improve disturbance rejection performance. In fact, this concept is not demonstrated in other control systems.

Finally, several comparative simulations of a nonlinear six-DOF UPH system were conducted to evaluate the performance of the proposed control scheme.

The remainder of this paper is organized as follows: Section 2 presents a dynamic model of the UPH system. The design process for the proposed TSMC, the predefined-time control, and the prescribed-performance control are presented in Section 3. The simulation results for the UPH model are presented in Section 4. Finally, the conclusions of this study are presented in Section 5.

2. Modeling the UPH

A simplified UPH system with a characteristic porpoising motion is shown in Figure 1 [48], where the UPH system features six-DOF motion, and the definitions of the coordinate variables are presented in Table 1.

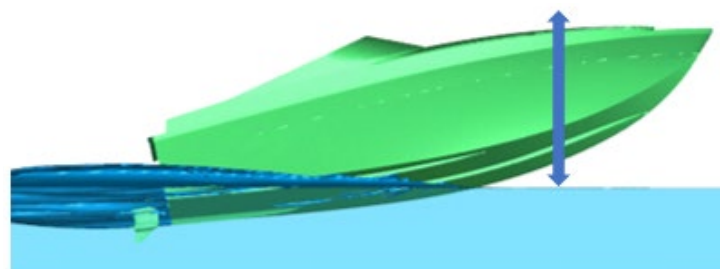


Figure 1. Simple shape of UPH and porpoising motion.

Table 1. Definitions of each coordinate variable.

Nomenclature	Force and Moment	Linear and Rotary Velocity	Position and Euler Angle
Surge	X	u	x
Sway	Y	v	y
Heave	Z	w	z
Roll	K	p	ϕ
Pitch	M	q	θ
Yaw	N	r	ψ

2.1. Dynamics of UPH

The kinematics of the UPH between the inertial and body coordinated frames are expressed as follows:

$$\begin{aligned} \dot{\eta}_1 &= J_1(\eta_2)v_1 \\ \dot{\eta}_2 &= J_2(\eta_2)v_2 \end{aligned} \tag{1}$$

where

$$\eta = \begin{bmatrix} \eta_1 \\ \eta_2 \end{bmatrix} \quad \eta_1 = \begin{bmatrix} x \\ y \\ z \end{bmatrix} \quad \eta_2 = \begin{bmatrix} \phi \\ \theta \\ \psi \end{bmatrix} \quad v = \begin{bmatrix} v_1 \\ v_2 \end{bmatrix} \quad v_1 = \begin{bmatrix} u \\ v \\ w \end{bmatrix} \quad v_2 = \begin{bmatrix} p \\ q \\ r \end{bmatrix}$$

$$J_1(\eta_2) = \begin{bmatrix} c\psi c\theta & -s\psi c\phi + c\psi s\theta s\phi & s\psi s\phi + c\psi c\phi s\theta \\ s\psi c\theta & c\psi c\phi + s\phi s\theta s\psi & -c\psi s\phi + s\theta s\psi c\phi \\ -s\theta & c\theta s\phi & c\theta c\phi \end{bmatrix}$$

$$J_2(\eta_2) = \begin{bmatrix} 1 & s\phi t\theta & c\phi t\theta \\ 0 & c\phi & -s\phi \\ 0 & s\phi/c\theta & c\phi/c\theta \end{bmatrix}$$

The six-DOF nonlinear rigid body dynamics of the UPH are expressed as follows:

$$M_{RB}v + C_{RB}(v)v = \Gamma_{RB}, \tag{2}$$

where $v = [u \ v \ w \ p \ q \ r]^T$. M_{RB} denotes the inertia matrix of the rigid body, which can be represented by

$$M_{RB} = \begin{bmatrix} m & 0 & 0 & 0 & mz_g & -my_g \\ 0 & m & 0 & -mz_g & 0 & mx_g \\ 0 & 0 & m & my_g & -mx_g & 0 \\ 0 & -mz_g & my_g & I_x & -I_{xy} & -I_{xz} \\ mz_g & 0 & -mx_g & -I_{yx} & I_y & -I_{yz} \\ -my_g & mx_g & 0 & -I_{zx} & -I_{zy} & I_z \end{bmatrix} \tag{3}$$

$C_{RB}(v)$ denotes the Coriolis centripetal matrix, which can be represented by

$$C_{RB}(v) = \begin{bmatrix} 0 & 0 & 0 \\ 0 & 0 & 0 \\ 0 & 0 & 0 \\ -m(y_g q + z_g r) & m(y_g p + w) & m(z_g p - v) \\ m(x_g q - w) & -m(z_g r + x_g p) & m(z_g q + u) \\ m(x_g r + v) & m(y_g r - u) & -m(x_g p + y_g q) \end{bmatrix}$$

$$\begin{bmatrix} m(y_g q + z_g r) & -m(x_g q - w) & m(x_g r + v) \\ -m(y_g p + w) & m(z_g r + x_g p) & -m(y_g r - u) \\ -m(z_g p - v) & -m(z_g q + u) & m(x_g p + y_g q) \\ 0 & -I_{yz}q - I_{xz}p + I_z r & I_{yz}r + I_{xy}p - I_y q \\ I_{yz}q + I_{xz}p - I_z r & 0 & -I_{xy}r - I_{xy}q + I_x p \\ -I_{yz}r - I_{xy}p + I_y q & I_{xy}r + I_{xy}q - I_x p & 0 \end{bmatrix} \quad (4)$$

$\Gamma_{RB} = \Gamma + \Gamma_H + \Gamma_E$ is the generalized force and moment vector, Γ denotes the propulsion and moment vector, Γ_H denotes the hydraulic force and moment vector, and Γ_E denotes the environmental disturbance vector, which is composed of the current, wave, and wind disturbance vectors, i.e., $\Gamma_E = \Gamma_E^{current} + \Gamma_E^{wave} + \Gamma_E^{wind}$.

2.2. The Modeling of the Drag Force and Pitching Moment of the UPH

The weight of the UPH is supported by the hydraulic pressure generated by the ship body under high-speed navigation conditions. This pressure is transformed into a lift force exerting on the body of the ship, thus resulting in a decrease in resistance. Estimating resistance experimentally is very difficult because the hydraulic equation to be used contains many unknown hydraulic and disturbance parameters. The Savisky method [1] can be used to calculate the resistance and pitching-moment variation based on the variation in the trim angle via an analysis of the fluid field of the planing side. A schematic representation of the UPH is shown in Figure 2 and the semantics of the UPH parameters of Figure 2 are listed in Table 2.

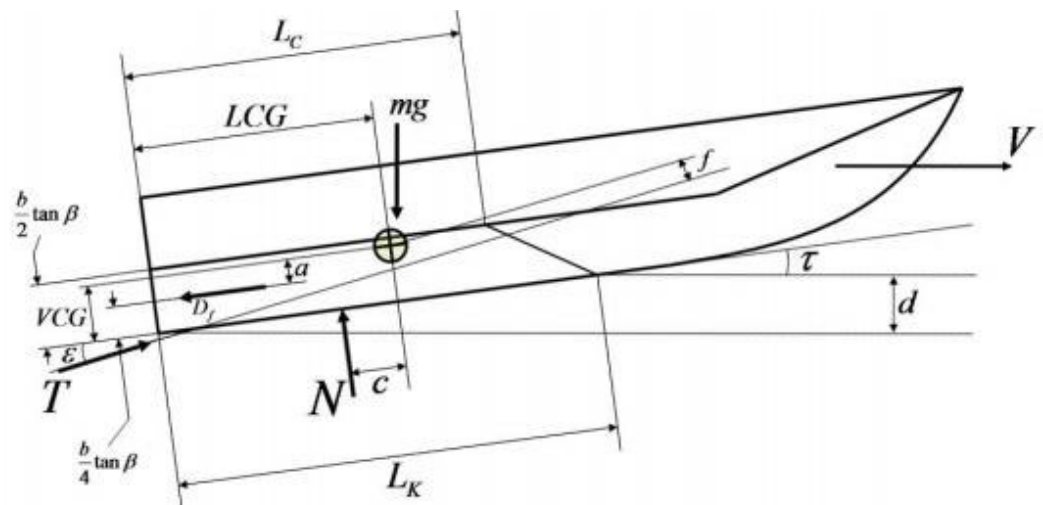


Figure 2. Schematic illustration of UPH.

Table 2. Dimensional and dynamic symbols and corresponding semantics of UPH.

Symbol	Semantics
LCG	the longitudinal distance from the transom to the center of gravity
VCG	the perpendicular distance for the bottom from keel to the center of gravity
N, T	the vertical drag force and the propulsion force of the propeller
D_f	the viscous friction drag of the body
f, c	the distance between T, N , and the center of gravity, respectively
d, τ, b	the draft of the keel in the transom, the trim angle of keel, and the chine width
a, V	The distance between D_f and the center of gravity, and the speed of the boat
ϵ	the angle between the propulsion force and trim line
β, Δ	the inclination angle of the planing side and the weight of the body
L_C, L_k	the flooded length of the chine and the flooded length of keel

The vertical drag (normal force) N is expressed as

$$N = \frac{\Delta}{\cos \tau} \tag{5}$$

D_f denotes the friction drag (tangential force). The dynamic equations for a general planing hull where the force does not pass the center of gravity are expressed as follows:

$$(T \cos(\tau + \varepsilon) - N \sin \tau - D_f \cos \tau)\mathbf{i} + (N \cos \tau + T \sin(\tau + \varepsilon) - mg - D_f \sin \tau)\mathbf{j} = 0 \tag{6}$$

$$(N \times c + D_f \times a - T \times f)\mathbf{k} = 0 \tag{7}$$

The friction drag D_f exerted on the body skin as a tangential force and the vertical force N exerted on the floor of the body at the center point of the weight of the body generate the bow-down moment, where the effective lever arms correspond to c and a , respectively. Meanwhile, the propulsion force T generated from the propeller generates a bow-up moment, where the effective lever arm corresponds to f . Assuming a small τ , we can obtain the following from (6):

$$T \cos \varepsilon = \Delta \sin \tau + D_f \tag{8}$$

Next, assuming that $\cos \varepsilon \approx 1$ in (8) and substituting it into (6), we obtain

$$\begin{aligned} \Delta &= N \cos \tau + \Delta \sin \tau \sin(\tau + \varepsilon) + D_f \sin(\tau + \varepsilon) - D_f \sin \tau \\ &\approx N \cos \tau + \Delta \sin \tau \sin(\tau + \varepsilon) \end{aligned} \tag{9}$$

Subsequently, we obtain

$$N = \frac{\Delta[1 - \sin \tau \sin(\tau + \varepsilon)]}{\cos \tau} \tag{10}$$

$$T = \frac{\Delta \sin \tau + D_f}{\cos \varepsilon} \approx \Delta \sin \tau + D_f \tag{11}$$

Considering (7), (10), and (11), the total moment can be expressed as follows:

$$M_{tot} = \Delta \left[\frac{c}{\cos \tau} (1 - \sin \tau \sin(\tau + \varepsilon)) - f \sin \tau \right] + D_f(a - f) \tag{12}$$

where the lever arms are expressed as

$a = VCG - \frac{b}{4} \tan \beta$, VCG = the vertical distance between the transom and center of weight,

$$c = LCG - l_p,$$

l_p = the distance between the transom and the vertical force exerted based on the keel.

The equilibrium moment implies that $M_{tot} = 0$. If a negative moment is observed, then the assumed navigation trim value is extremely low. The navigation trim is an extremely important factor and, thus, should be estimated appropriately because it determines the high-speed navigation performance. An inaccurate trim causes unstable motion, such as porpoising motion, i.e., the dolphin phenomenon, during navigation. In actual applications, the trim angle, engine power, and size of the flooded chine and keel should be selected such that the pitching-moment becomes zero. Otherwise, the equilibrium moment condition is violated and a disturbance pitching moment may be generated.

Therefore, considering the drag force and pitching moment derived in the previous section, the generalized external force and moment in the six-DOF rigid body dynamics of the UPH can be expressed as follows:

$$\mathbf{I}_{RB} = \mathbf{I} + \mathbf{I}_H \tag{13}$$

where

$$\Gamma = [u_u \ 0 \ 0 \ 0 \ 0 \ u_r]^T \Gamma_H = [D_u \ 0 \ 0 \ 0 \ D_q \ 0]^T$$

$$D_u = -mg \tan \tau - \frac{D_f}{\cos \tau}$$

$$D_q = -M_{tot} = -\Delta \left[\frac{c}{\cos \tau} (1 - \sin \tau \sin(\tau + \varepsilon)) - f \sin \tau \right] - D_f(\alpha - f)$$

u_u, u_r denote the control inputs for the surge and yaw axes, D_u denotes the resistance in the surge axis, and D_q denotes the pitching moment, respectively.

Remark 1. The pitching moment D_q as shown in (14) is separated from the control input u_r along the yaw axis, as shown in (15):

$$I_y \dot{q} = -m [-(\dot{w} + vp - uq)x_g + (\dot{u} - vr + wq)z_g] - [I_y \dot{q} + (I_x - I_z)pr - I_{yz}\dot{r} + (I_{yz}p - I_{xy}r)q + I_{xz}(p^2 - r^2)] - D_q \tag{14}$$

$$I_z \dot{r} = m [(\dot{v} + ur - wp)x_g - (\dot{u} - vr + wq)y_g] + [(-I_{xz}\dot{p} + I_{yz}\dot{q}) + (I_{xz}q - I_{yz}p)r + (I_y - I_x)pq + I_{xy}(q^2 - p^2)] + u_r \tag{15}$$

Thus, when this moment appears, compensating for the disturbance directly using a conventional disturbance observer based on the pitch or yaw axis dynamics is difficult owing to the underactuated UPH system. Therefore, other types of disturbance compensators are required.

2.3. Modeling the Rudder Hydraulic Actuator

The rudder mechanism is an actuator type in which the rudder rotary angle is determined based on the cylinder stroke of a hydraulic system, after which the rate of turn is obtained. The rudder hydraulic system was designed under the operating conditions of a single cylinder with a stroke and the maximum rudder saturation angle. The linear motion of the hydraulic cylinder was converted into rotary motion via the hinge of the rudder. The hydraulic system is composed of an oil pump, an orifice flow valve, and a cylinder. The cylinder velocity is controlled by the area of the orifice valve, and the position of the piston is determined by the pump flow as shown in Figure 3.

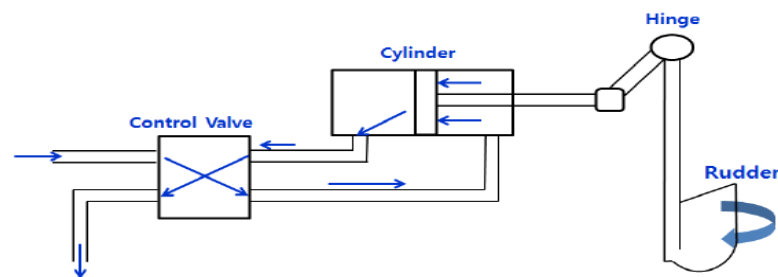


Figure 3. Mechanism of hydraulic rudder actuator.

The block diagram of the hydraulic rudder control system is shown in Figure 4.

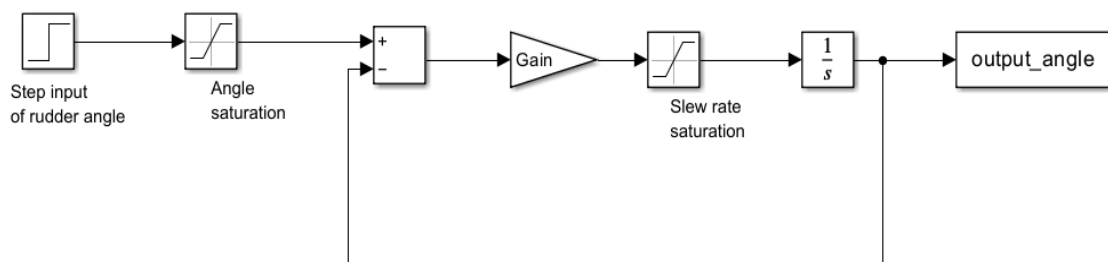


Figure 4. Mechanism of rudder controller.

The slew rate saturation is the maximum rotary velocity. The time delay of the rudder is expressed as

$$t_\delta = \frac{\dot{\delta}_{r\max}}{\delta_r} \tag{16}$$

where δ_r denotes the deflection of the rudder and $\dot{\delta}_{r\max}$ denotes the maximum rotary velocity of the rudder.

3. Controller Design of the UPH

3.1. Fundamentals Regarding Predefined-Time Stability and Prescribed-Performance Function

Consider the following system:

$$\dot{x}(t) = f(t, x; a) \tag{17}$$

where $x(t) \in R^n$ denotes the state of the system, $f : R \rightarrow R^n$ is a nonlinear function, and $a \in R^b$ denotes the constant system parameters. The time t is bounded by the interval $[t_0, \infty)$, where $t_0 \geq 0$, and $x(t_0) = x_0$ denotes the initial state of the system.

Definition 1 [28]. The origin of system (17) is globally finite-time stable if it is globally asymptotic stable and any solution $x(t, x_0)$ of system (17) reaches the equilibrium point at some finite time moment, i.e., $\forall t \geq T(x_0): x(t, x_0) = 0$, where $T : R^n \rightarrow R_+ \cup \{0\}$.

Definition 2 [28]. The origin of system (17) is fixed-time stable if the origin of system (17) exhibits finite-time stability and the settling-time function is bounded, i.e., $\exists T_{\max} \geq 0 : T(x_0) \leq T_{\max} \cdot \forall x_0$.

Definition 3 [28]. In the case of fixed-time stability, the origin of system (17) exhibits predefined-time stability if the parameter $a \in R^b$ of system (17) can be selected such that the settling-time function T_{\max} can be predefined as desired.

Definition 4 [28]. For $x(t) \in R^n$, the predefined-time stabilizing function is defined as follows:

$$\varphi_p(x; T_c) = \frac{1}{pT_c} \exp(x^p) |x|^{1-p} \tag{18}$$

where $T_c > 0$, $0 < p \leq 1$, and $\dot{\varphi}_p = \frac{d\varphi_p}{dt}$ exists for all x and T_c .

Lemma 1 [28]. For every initial condition x_0 , the following system is globally and strongly predefined-time stable under a strongly predefined time T_c :

$$\dot{x}(t) = -\varphi_p(x; T_c) \tag{19}$$

This implies that $x(t) = 0$ holds for all $t \geq t_0 + T_c$, regardless of the value of x_0 . A smooth decreasing function $\rho(t) > 0$ is defined as follows:

$$\rho(t) = (\rho_0 - \rho_{ss})e^{-a_r t} + \rho_{ss} \tag{20}$$

where $\rho_0, \rho_{ss} = \lim_{t \rightarrow \infty} \rho(t)$, and a_r denote the positive constants selected for the confining error bound. The heading-angle tracking error is guaranteed to remain in the prescribed transient and steady-state range bounds as follows:

$$-\rho(t) < e_r(t) < \rho(t) \tag{21}$$

The transformed constraint error is selected as follows [42]:

$$\zeta_r(t) = \frac{e_r(t)}{\rho(t)} \tag{22}$$

The error transformation is selected as follows [42]:

$$\Lambda_{pr}(t) = \tan(\kappa_r \zeta_r(t)) \tag{23}$$

where $\Lambda_{pr}(t)$ denotes a smooth and strictly bounded function and $0 < \kappa_r < \pi/2$.

Theorem 1. *The following condition is true if and only if ρ_0, ρ_{ss} , and a are selected as positive constants, such that (21) is satisfied.*

$$0 \leq \Lambda_{pr}(t) \leq \tan(\kappa_r), \quad \forall t > 0 \tag{24}$$

Proof of Theorem 1. See the proof in Theorem 1 [42]. □

3.2. Predefined-Time TSMC Controller Design for Surge Velocity

The target velocity $\lim_{t \rightarrow \infty} U \rightarrow U_d$ as $t \rightarrow \infty$. Furthermore, $u \rightarrow \sqrt{U_d^2 - v^2}$ because $U = \sqrt{u^2 + v^2}$. The desired surge velocity can be expressed as $u_d \rightarrow \sqrt{U_d^2 - v^2}$ because $U_d \geq |v|$ is always satisfied. In actual scenarios, the aim of surge control is $\lim_{t \rightarrow \infty} u \rightarrow u_d$ because $|v|$ occupies a small portion in $U = \sqrt{u^2 + v^2}$. To facilitate controller design, the cross-product of inertia terms is disregarded, i.e., $I_{xy} = I_{zx} = I_{zy} = I_{yz} = 0$. Hence, the surge dynamics described in (2) and (13) can be rewritten as follows:

$$\dot{u} = f_u + \frac{1}{m}u_u + d_u \tag{25}$$

where $d_u = \frac{1}{m}D_u, |d_u| \leq \Delta_u$, and Δ_u denote the unknown disturbance bound, and

$$f_u = -[-vr + wq - x_g(q^2 + r^2) + y_g(-\dot{r} + pq) + z_g(\dot{q} + pr)] \tag{26}$$

A surge velocity error is defined as $e_u = u_d - u$, and a sliding surface is defined as

$$\sigma_u = e_u + \int_0^t (k_{u1}e_u + k_{u2}sig^{1/2}(e_u))dt \tag{27}$$

where $k_{ui} > 0, i = 1, 2$, are constants. Taking the time derivative of (27), we obtain

$$\begin{aligned} \dot{\sigma}_u &= \dot{e}_u + (k_{u1}e_u + k_{u2}sig^{1/2}(e_u)) \\ &= \dot{u}_d - f_u - \frac{1}{m}u_u - d_u + (k_{u1}e_u + k_{u2}sig^{1/2}(e_u)) \end{aligned} \tag{28}$$

The control input is selected as follows:

$$u_u = m(u_{ueq} + u_{urob} + u_{upt}) \tag{29}$$

$$u_{ueq} = c_{u1}\sigma_u + c_{u2}sig^{1/2}(\sigma_u) + \dot{u}_d - f_u + k_{u1}e_u + k_{u2}sig^{1/2}(e_u) \tag{30}$$

$$u_{urob} = c_{u3} \frac{\sigma_u}{|\sigma_u| + \varepsilon_u} \tag{31}$$

$$u_{upt} = \frac{1}{(\sqrt{2})^{\gamma_u+1} p_u T_{cu}} \exp(V_1^{p_u}) sig^{\gamma_u}(\sigma_u) \tag{32}$$

where $c_{ui} > 0, i = 1, 2, 0 < \varepsilon_u \leq 1, 0 < p_u \leq 1$, and $0 < \gamma_u < 1$ are constants. The Lyapunov function candidate is defined as follows:

$$V_1 = \frac{1}{2}\sigma_u^2 \tag{33}$$

Applying the time derivative to (33) and considering (29) yields

$$\begin{aligned}
 \dot{V}_1 &= \sigma_u \dot{\sigma}_u \\
 &= \sigma_u \left[\dot{u}_d - f_u - \frac{1}{m} u_u - d_u + k_{u1} e_u + k_{u2} \text{sig}^{1/2}(e_u) \right] \\
 &= \sigma_u \left(-c_{u1} \sigma_u - c_{u2} \text{sig}^{1/2}(\sigma_u) - c_{u2} \frac{\sigma_u}{|\sigma_u| + \varepsilon_u} - d_u \right. \\
 &\quad \left. - \frac{1}{(\sqrt{2})^{\gamma_u+1} p_u T_{cu}} \exp(V_1^{p_u}) \text{sig}^{\gamma_u}(\sigma_u) \right) \\
 &\leq -c_{u2} \frac{\sigma_u^2}{|\sigma_u| + \varepsilon_u} - \frac{1}{(\sqrt{2})^{\gamma_u+1} p_u T_{cu}} \exp(V_1^{p_u}) \text{sig}^{\gamma_u+1}(\sigma_u) + |\sigma_u| \Delta_u \\
 &\leq -|\sigma_u| \left(\frac{c_{u2} |\sigma_u|}{|\sigma_u| + \varepsilon_u} - \Delta_u \right) - \frac{1}{(\sqrt{2})^{\gamma_u+1} p_u T_{cu}} \exp(V_1^{p_u}) \text{sig}^{\gamma_u+1}(\sigma_u)
 \end{aligned} \tag{34}$$

If c_{u2} is selected such that the condition of $\frac{c_{u2} |\sigma_u|}{|\sigma_u| + \varepsilon_u} \geq \Delta_u$ is satisfied, and considering the result of $\sqrt{2} V_1 \leq |\sigma_u|^{\gamma_u+1}$ [8], then (34) can be expressed as follows:

$$\begin{aligned}
 \dot{V}_1 &\leq -\frac{1}{(\sqrt{2})^{\gamma_u+1} p_u T_{cu}} \exp(V_1^{p_u}) (2V_1)^{(\gamma_u+1)/2} \\
 &\leq -\frac{1}{p_u T_{pu}} \exp(V_1^{p_u}) V_1^{(\gamma_u+1)/2}
 \end{aligned} \tag{35}$$

where $(\sqrt{2})^{\gamma_u+1} T_{cu} = T_{pu}$. By setting $\gamma_u = 1 - 2p_u$, we obtain

$$\dot{V}_1 \leq -\frac{1}{p_u T_{pu}} \exp(V_1^{p_u}) V_1^{1-p_u} \tag{36}$$

Based on the result of Lemma 1, $\sigma_u \rightarrow 0$ can be achieved in a predefined time T_{pu} of the surge axis, which is expressed as

$$T_u \leq T_{pu} \tag{37}$$

Remark 2. The TSMC system is designed using (29) by removing the predefined-time control term, as follows:

$$u_u = m(u_{ueq} + u_{urob}) \tag{38}$$

3.3. Predefined-Time Second-Order TSMC System Design for Heading Angle

The yaw axis dynamics can be rewritten to facilitate the TSMC system’s design by disregarding the small cross-product of the inertia terms as follows

$$\dot{r} = f_r(u, v, w, p, q) + \frac{x_\delta P_u}{I_z} \delta_r + d_r \tag{39}$$

where x_δ denotes the moment arm length from the center of rotation for the pivot point of propulsion, d_r denotes the disturbance in the heading axis, P_u denotes the propulsion in the surge axis, and δ_r denotes the rudder angle. Meanwhile, the coupled nonlinear dynamics of the heading axis is expressed as follows:

$$f_r(u, v, w, p, q) = \frac{m}{I_z} [(\dot{v} + ur - wp)x_g - (\dot{u} - vr + wq)y_g] + \frac{1}{I_z} (I_y - I_x)pq \tag{40}$$

As shown in Figure 3, a first-order delay occurred in the angle-position output of the rudder actuator. This delay can be expressed using the following transfer function:

$$G(s) = \frac{\delta_r}{u_r} = \frac{1}{t_d s + 1} \tag{41}$$

where u_r is the control input for the rudder angle and t_d is the time constant. The state space model of (41) can be expressed as

$$\tau \dot{\delta}_r + \delta_r = u_r \tag{42}$$

or

$$\dot{\delta}_r = -(1/t_d)\delta_r + (1/t_d)u_r \tag{43}$$

Taking the time derivative of (39) and considering (42), we obtain

$$\begin{aligned} \ddot{r} &= \dot{f}_r(\dot{u}, \dot{v}, u, v, w, p, q) + \frac{x_\delta P_u}{I_z} \dot{\delta}_r + \dot{d}_r \\ &= F_r(\dot{u}, \dot{v}, u, v, w, p, q, \delta_r) + \frac{x_\delta P_u}{t_d I_z} u_r + \dot{d}_r \end{aligned} \tag{44}$$

where

$$\begin{aligned} F_r(\dot{u}, \dot{v}, u, v, w, p, q, \delta_r) &= \frac{\partial f_r}{\partial \dot{u}} \ddot{u} + \frac{\partial f_r}{\partial \dot{v}} \ddot{v} + \frac{\partial f_r}{\partial u} \dot{u} + \frac{\partial f_r}{\partial v} \dot{v} + \frac{\partial f_r}{\partial w} \dot{w} + \frac{\partial f_r}{\partial p} \dot{p} + \frac{\partial f_r}{\partial q} \dot{q} - \frac{x_\delta P_u}{t_d I_z} \delta_r \\ \frac{\partial f_r}{\partial \dot{u}} &= -\frac{m y_g}{I_z} \frac{\partial f_r}{\partial \dot{v}} = \frac{m x_g}{I_z} \frac{\partial f_r}{\partial u} = \frac{m x_g r}{I_z} \frac{\partial f_r}{\partial v} = \frac{m y_g r}{I_z} \frac{\partial f_r}{\partial w} = -\frac{m x_g}{I_z} \\ \frac{\partial f_r}{\partial p} &= -\frac{m x_g}{I_z} w + \frac{1}{I_z} (I_x - I_y) q \quad \frac{\partial f_r}{\partial q} = -\frac{m y_g}{I_z} w + \frac{1}{I_z} (I_x - I_y) p \end{aligned}$$

To simplify the dynamics, we disregard w - and q -axis terms with insignificant contributions, which yields the following expression:

$$F_r(\dot{u}, \dot{v}, p, \delta_r) = \frac{m}{I_z} [x_g(\ddot{v} + r\dot{u}) + y_g(-\ddot{u} + r\dot{v})] - \frac{x_\delta P_u}{t_d I_z} \delta_r \tag{45}$$

Subsequently, we define the errors of the heading axis as follows:

$$\begin{aligned} e_r &= \psi_d - \psi \\ \dot{e}_r &= \dot{\psi}_d - \dot{\psi} = r_d - r \\ \ddot{e}_r &= \ddot{\psi}_d - \ddot{\psi} = \dot{r}_d - \dot{r} \end{aligned} \tag{46}$$

Thus, the second-order sliding mode surface is expressed as follows:

$$\sigma_r = \ddot{e}_r + k_{r2} sig^{\alpha_2}(\dot{e}_r) + k_{r1} sig^{\alpha_1}(e_r) \tag{47}$$

In (47), α_1 and α_2 are selected as [49]

$$\begin{cases} \alpha_2 = \alpha \in (1 - \varepsilon, 1), \quad \varepsilon \in (0, 1) \\ \alpha_1 = \frac{\alpha_2 \alpha_3}{2\alpha_3 - \alpha_2}, \quad \alpha_3 = 1 \end{cases} \tag{48}$$

The coefficient $c_{ri} > 0$ is selected such that the polynomial $p^2 + k_r p + k_{r1}$ is Hurwitz. Taking the time derivative of (47) and considering (45) and (46), we obtain

$$\begin{aligned} \dot{\sigma}_r &= \ddot{e}_r + k_{r2}\alpha_2|\dot{e}_r|^{\alpha_2-1}\ddot{e}_r + k_{r1}\alpha_1|e_r|^{1-\alpha_1}\dot{e}_r \\ &= \ddot{r}_d + k_{r2}\alpha_2|\dot{e}_r|^{\alpha_2-1}\ddot{e}_r + k_{r1}\alpha_1|e_r|^{1-\alpha_1}\dot{e}_r - F_r(\dot{u}, \dot{v}, p, \delta_r) - \frac{x_\delta P_u}{t_d I_z} u_r - \dot{d}_r \end{aligned} \tag{49}$$

The heading control law is selected as follows:

$$u_r = \frac{t_d I_z}{x_\delta P_u} (u_{req} + u_{rrob} + u_{rpt}) \tag{50}$$

$$u_{req} = c_{r1}\sigma_r + c_{r2}sig^{1/2}(\sigma_r) + \ddot{r}_d - k_{r2}\alpha_2|\dot{e}_r|^{\alpha_2-1}\ddot{e}_r - k_{r1}\alpha_1|e_r|^{1-\alpha_1}\dot{e}_r + F_r(\dot{u}, \dot{v}, p, \delta_r) \tag{51}$$

$$u_{rrob} = c_{r3} \frac{\sigma_r}{|\sigma_r| + \varepsilon_r} \tag{52}$$

$$u_{rpt} = \frac{1}{(\sqrt{2})^{\gamma_r+1} p_r T_{cr}} \exp(V_2^{p_r}) sig^{\gamma_r}(\sigma_r) \tag{53}$$

where $c_{ri} > 0$, $i = 1, 2, 3$, $0 < \varepsilon_r \leq 1$, $0 < p_r \leq 1$, and $0 < \gamma_r < 1$ are constants. Defining the Lyapunov function candidate as

$$V_2 = \frac{1}{2} \sigma_r^2 \tag{54}$$

and taking its time derivative in addition to considering (50), we obtain

$$\begin{aligned} \dot{V}_2 &= \sigma_r \dot{\sigma}_r \\ &\leq \sigma_r \left(\ddot{r}_d + k_{r2}\alpha_2|\dot{e}_r|^{\alpha_2-1}\ddot{e}_r + k_{r1}\alpha_1|e_r|^{1-\alpha_1}\dot{e}_r - F_r(\dot{u}, \dot{v}, p, \delta_r) - \frac{x_\delta P_u}{t_d I_z} u_r + \Delta_r \right) \end{aligned} \tag{55}$$

where $|\dot{d}_r| \leq \Delta_r$. Substituting (50) into (55), we obtain

$$\begin{aligned} V_2 &\leq -c_{r2}|\sigma_r|^{3/2} - c_{r3} \frac{\sigma_r^2}{|\sigma_r| + \varepsilon_r} - \frac{1}{(\sqrt{2})^{\gamma_r+1} p_r T_{cr}} \exp(V_2^{p_r}) sig^{\gamma_r+1}(\sigma_r) + |\sigma_r| |\dot{d}_r| \\ &\leq -|\sigma_r| \left(\frac{c_{r3}|\sigma_r|}{|\sigma_r| + \varepsilon_r} - \Delta_r \right) - \frac{1}{(\sqrt{2})^{\gamma_r+1} p_r T_{cr}} \exp(V_2^{p_r}) sig^{\gamma_r}(\sigma_r) \end{aligned} \tag{56}$$

If c_{r2} is selected such that the condition $\frac{c_{r3}|\sigma_r|}{|\sigma_r| + \varepsilon_r} \geq \Delta_r$ is satisfied and considering the result of $\sqrt{2V_2} \leq |\sigma_r|^{\gamma_r+1}$ [8], then (56) can be expressed as follows:

$$\begin{aligned} \dot{V}_2 &\leq -\frac{1}{(\sqrt{2})^{\gamma_r+1} p_r T_{cr}} \exp(V_2^{p_r}) (2V_2)^{(\gamma_r+1)/2} \\ &\leq -\frac{1}{p_r T_{pr}} \exp(V_2^{p_r}) V_2^{(\gamma_r+1)/2} \end{aligned} \tag{57}$$

where $(\sqrt{2})^{\gamma_r+1} T_{cr} = T_{pr}$. By setting $\gamma_r = 1 - 2p_r$, we obtain

$$\dot{V}_2 \leq -\frac{1}{p_r T_{pr}} \exp(V_2^{p_r}) V_2^{1-p_r} \tag{58}$$

Based on the result of Lemma 1, $\sigma_r \rightarrow 0$ can be achieved in a predefined time T_{pr} of the heading axis, which is expressed as

$$T_r \leq T_{pr} \tag{59}$$

Remark 3. The TSMC system is designed using (50) by removing the predefined-time control term as follows:

$$u_r = \frac{t_d I_z}{x_\delta P_u} (u_{req} + u_{rrob}) \tag{60}$$

3.4. Predefined-Time and Prescribed-Performance Second-Order TSMC System Design for Suppressing the Disturbance of the Heading Angle

The heading control law with predefine-time and prescribed-performance control terms is selected as follows:

$$u_r = \frac{t_d I_z}{x_\delta P_u} (u_{req} + u_{rrob} + u_{rpt} + u_{rpr}) \tag{61}$$

$$u_{rpr} = -c_{r4} \Lambda_{pr}(t) (\sigma_r + sig^{1/2}(\sigma_r)) \tag{62}$$

where $c_{r4} > 0$ is a constant. Substituting (61) into (55) and based on Theorem 1, we obtain

$$\begin{aligned} V_2 &\leq -c_{r2} |\sigma_r|^{3/2} - c_{r3} \frac{\sigma_r^2}{|\sigma_r| + \epsilon_r} - \frac{1}{(\sqrt{2})^{\gamma_r+1} p_r T_{cr}} \exp(V_2^{p_r}) sig^{\gamma_r+1}(\sigma_r) \\ &\quad - c_{r4} \Lambda_{pr}(t) \sigma_r^2 - c_{r4} |\sigma_r|^{3/2} + |\sigma_r| \left| \dot{d}_r \right| \\ &\leq -|\sigma_r| \left(\frac{c_{r3} |\sigma_r|}{|\sigma_r| + \epsilon_r} - \Delta_r \right) - \frac{1}{(\sqrt{2})^{\gamma_r+1} p_r T_{cr}} \exp(V_2^{p_r}) sig^{\gamma_r}(\sigma_r) \end{aligned} \tag{63}$$

Repeating the procedures outlined in (56)–(58), the predefined-time condition in (59) can also be obtained.

In this section, TSMC_1st is designed to control the surge velocity. Next, TSMC_2nd for the heading-angle control is designed to solve the issue of the input delay in the hydraulic actuator of the heading axis. Furthermore, predefined-time and prescribed-performance control schemes are adopted simultaneously in the TSMC systems to obtain faster tracking performance and compensate for the disturbance caused by the pitching moment. The closed-loop stabilities for the designed control systems are proved explicitly using the Lyapunov functions.

4. Simulation Results and Discussion

Simulations were performed to demonstrate the effectiveness of the proposed control strategy for a small UPH model. A small model of the UPH was designed based on a scale ratio of 1 : 6. The selected dynamics of the small UPH model system are listed in Table 3.

Table 3. Selected dynamics of small UPH model system.

Parameter	Value	Parameter	Value
m	20.8kg	f, c, d, a	0.026 m, 0.1 m, 0.12 m, 0.07 m
I_x, I_y, I_z	0.2 kgm ² , 0.452 kgm ² , 0.275 kgm ²	b, λ	0.71 m, 0.41
x_g, y_g, z_g	0.694 m, 0, 0.23 m	ϵ, β	4°, 10°
LCG, VCG	1.47 m, 0.11 m	τ, α	3°, 27.5°
ρ, C_f	1026 kg/m ³ , 0.8	A_w	0.21 m ²

The drag force in the surge axis was selected as follows:

$$D_u = 30.2u - 45 N \tag{64}$$

The tangential drag force is given by

$$D_f = \frac{1}{2} \rho V_m^2 A_w C_f \tag{65}$$

where A_w is the wetted surface, C_f is the friction drag coefficient, and the mean velocity of the running side is calculated as

$$V_m = u \left[1 - \frac{0.012\lambda^{1/2}\tau^{1.1} - 0.0065\beta(0.012\lambda^{1/2}\tau^{1.1})^{0.6}}{\lambda \cos \tau} \right]^{1/2} \tag{66}$$

The pitching moment can be generated from (13) by using the parameters in Table 3 and (66).

The slew rate saturation is the maximum rotary velocity, which was assumed as $\dot{\delta}_{r_{max}} = 10^\circ / \text{sec}$. A total time of 4.5 s was required to rotate the rudder angle plate by 30° (0.5236 rad), as shown in Figure 5a. The response velocity for the motion input of the rudder is expressed as shown in Figure 5b.

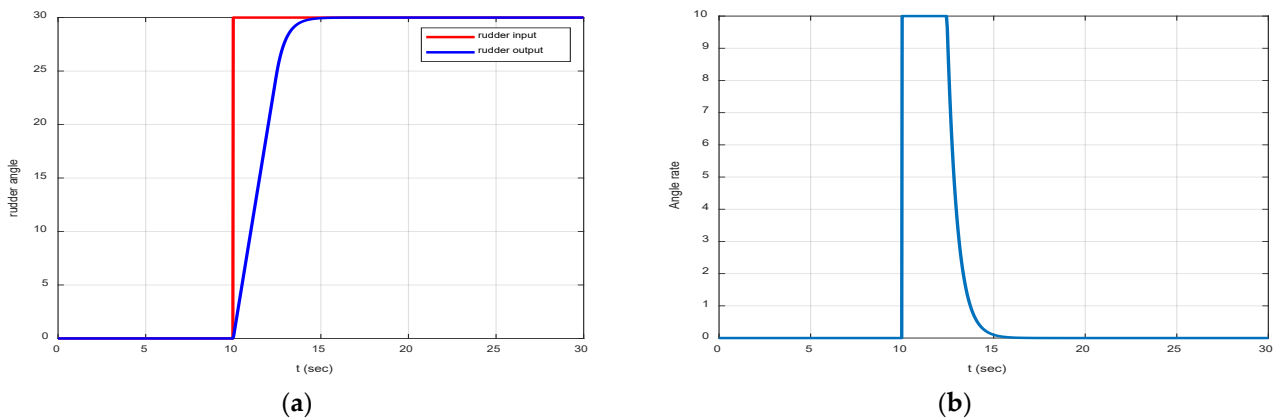


Figure 5. Time-delayed output angle and rudder slew rate for rudder input. (a) rudder angle; (b) angle rate.

Four control systems were designed to compare the performance of the proposed control strategy with the conventional strategy: first-order TSMC surge and heading controller (TSMC_1st), first-order TSMC surge controller and second-order TSMC heading controller (TSMC_2nd), first-order TSMC surge controller and second-order TSMC heading controller with the predefine-time control (PTSMC_2nd), and first-order TSMC surge controller and second-order TSMC heading controller with the predefine-time and prescribed-performance controls (P&PTSMC_2nd). The control parameters of the P&PTSMC_2nd system are listed in Table 4.

Table 4. Selected parameters of P&PTSMC system.

Parameter (Surge)	Value	Parameter (Heading)	Value
c_{u1}, c_{u2}, c_{u3}	2, 1.5, 1	$c_{r1}, c_{r2}, c_{r3}, c_{r4}, \kappa_r$	2, 1, 2, 10, 50
$k_{u1}, k_{u2}, \varepsilon_u$	1, 1.2, 0.01	$k_{r1}, k_{r2}, \varepsilon_r$	1, 1.25, 0.01
T_{cu}, p_u, γ_u	3, 0.2, 0.5	α_1, α_2	9/16, 9/23
		T_{cr}, p_r, γ_r	3, 0.05, 0.5
		ρ_0, ρ_{ss}, a_r	$30^\circ, 10^\circ, 0.5$

4.1. Simulation Results for the Step Command of Surge Velocity and Heading Angle

The simulation was performed to evaluate the control performance under the following step command inputs: surge velocity, 15 knots; heading angle 30° . The simulation results are shown in Figures 6 and 7. Figure 6 shows the surge velocity outputs and errors of the TSMC and PTSMC systems. Two cases for the PTSMC system were considered to show the faster response property of the predefined-time control, where the settling time of two PTSMC systems was shorter than that of the TSMC system owing to the predefined

control action. However, the PTSMC1 was selected in the next step because too fast a response in PTSMC2 causes the saturation of the surge control actuator of the propeller.

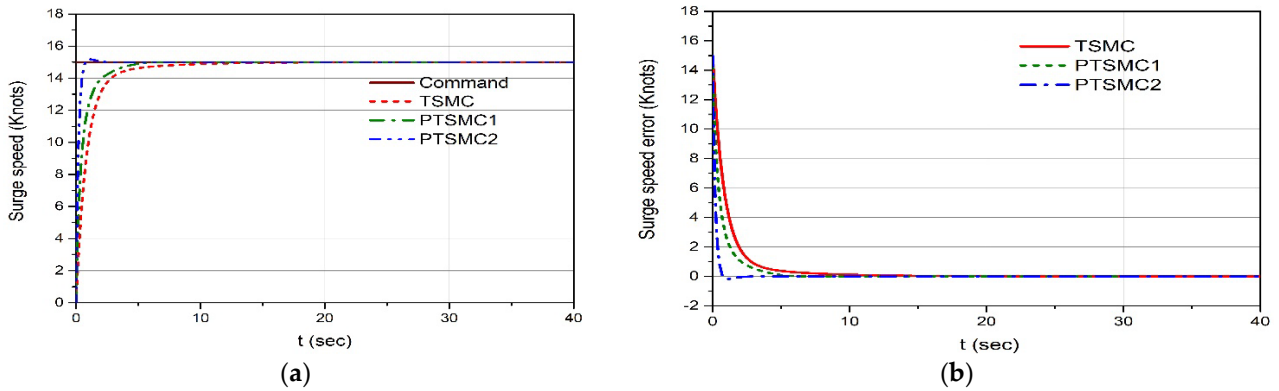


Figure 6. Time response for step surge velocity command: (a) surge velocity output; (b) surge velocity error.

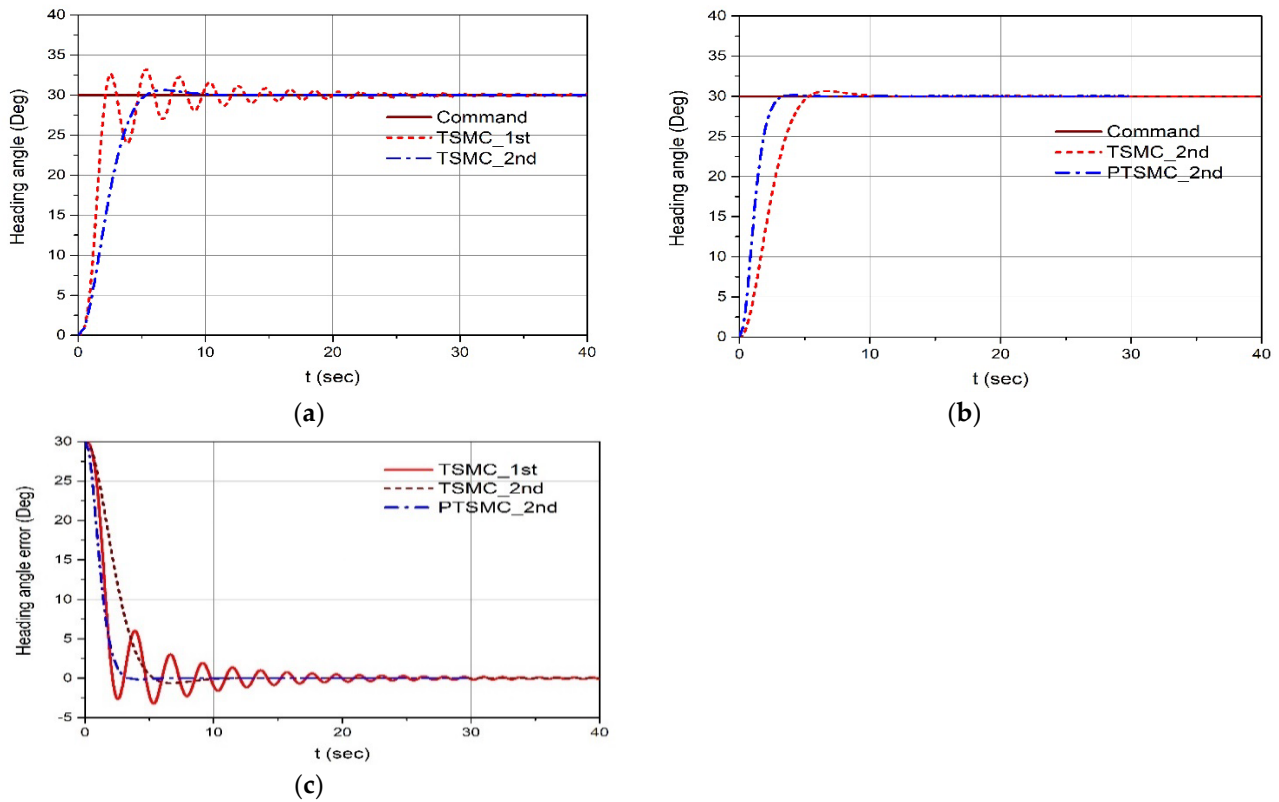


Figure 7. Time response for step heading-angle command under input delay: (a) heading-angle output of TSMC_1st and TSMC_2nd systems; (b) heading-angle output of TSMC_2nd and PTSMC_2nd systems; (c) heading-angle error of TSMC_1st, TSMC_2nd, and PTSMC_2nd systems.

The simulation results under an input delay in the heading control channel are shown in Figure 7. The TSMC_1st system exhibits severe oscillations because of the input delay effect, whereas the TSMC_2nd system exhibits a stable response because it considered the delay effect, as shown in Figure 7a. Meanwhile, the PTSMC_2nd system indicated a faster response owing to the predefined-time control action, as shown in Figure 7b. The tracking errors for three systems are shown in Figure 7c, where the PTSMC system showed the most stable and rapid response among the three systems.

4.2. Simulation Results for the Multi-Step Command of Surge Velocity and Sine Wave Heading Angle

The second simulation was performed to evaluate the control performance under multi-step command inputs comprising a surge velocity and a heading angle of $30^\circ \sin \omega t$ with $\omega = 0.157 \text{ rad/s}$. The simulation results are shown in Figures 8 and 9. Figure 8 shows the surge velocity outputs and errors of the TSMC and PTSMC systems under velocities of 10, 15, 20, and 25 knots. Similar to the previous result, the settling time of the PTSMC system was shorter than that of the TSMC system owing to the predefined-time control action, as shown in Figure 8b. Figure 8c shows the propulsion control inputs. The pulse control shapes were generated owing to step speed commands. This can be alleviated by smooth speed command in the real system's implementation.

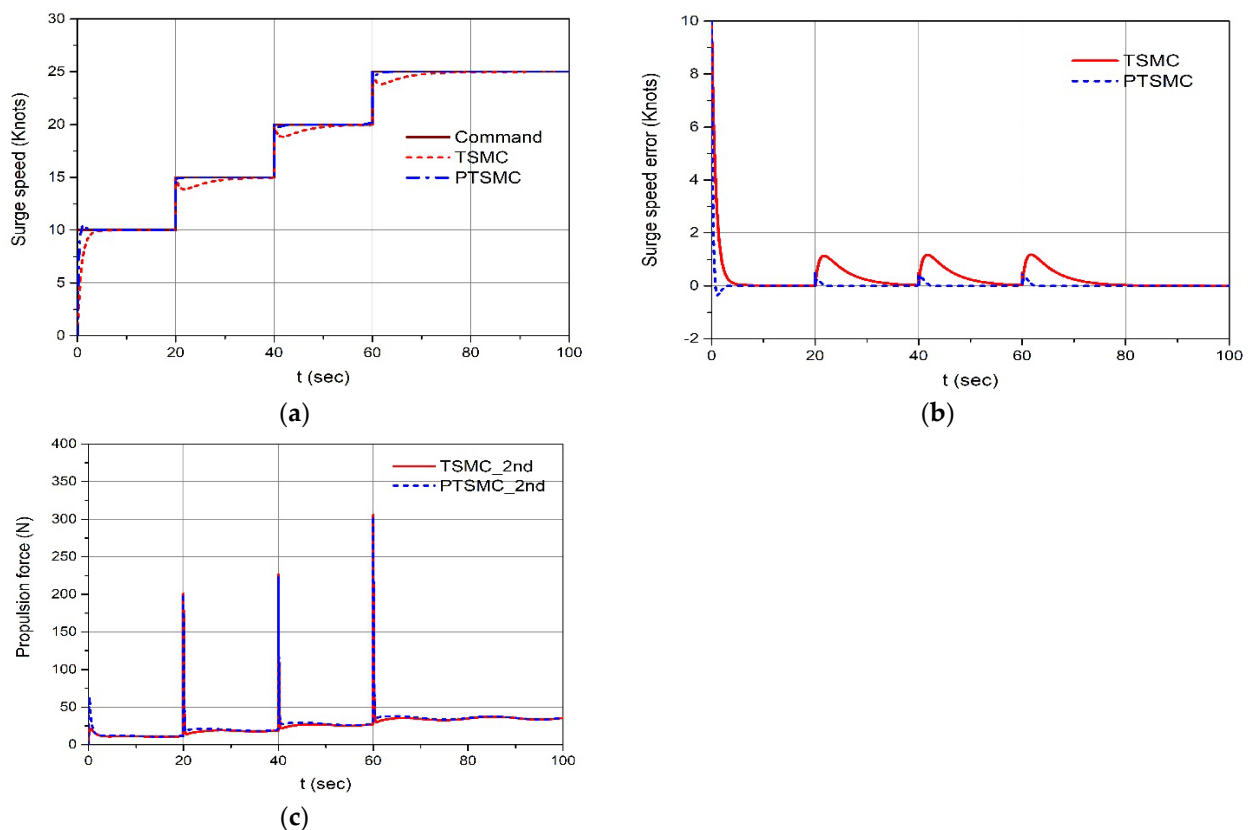


Figure 8. Time response and control input for multi-step surge velocity command of PTSMC_2nd and P&PTSMC_2nd systems: (a) surge velocity output; (b) surge velocity error; (c) propulsion force control input.

Figure 9 shows the heading-angle response for the sine wave commands of the TSMC_2nd and PTSMC_2nd systems. The tracking outputs are shown in Figure 9a, and the tracking errors are shown in Figure 9b, where the settling time of PTSMC_2nd is four times shorter than that of TSMC_2nd. As shown, the PTSMC system responded faster than the TSMC system, owing to the predefined-time control action. The rudder control angles of the two systems are shown in Figure 9c.

In this section, the tracking performance of the surge speed and heading angle for the multi-step surge speed command and the sinewave heading command is evaluated for the TSMC and PTSMC system. It was shown that the PTSMC system shows a faster tracking performance than that of the conventional TSMC system.

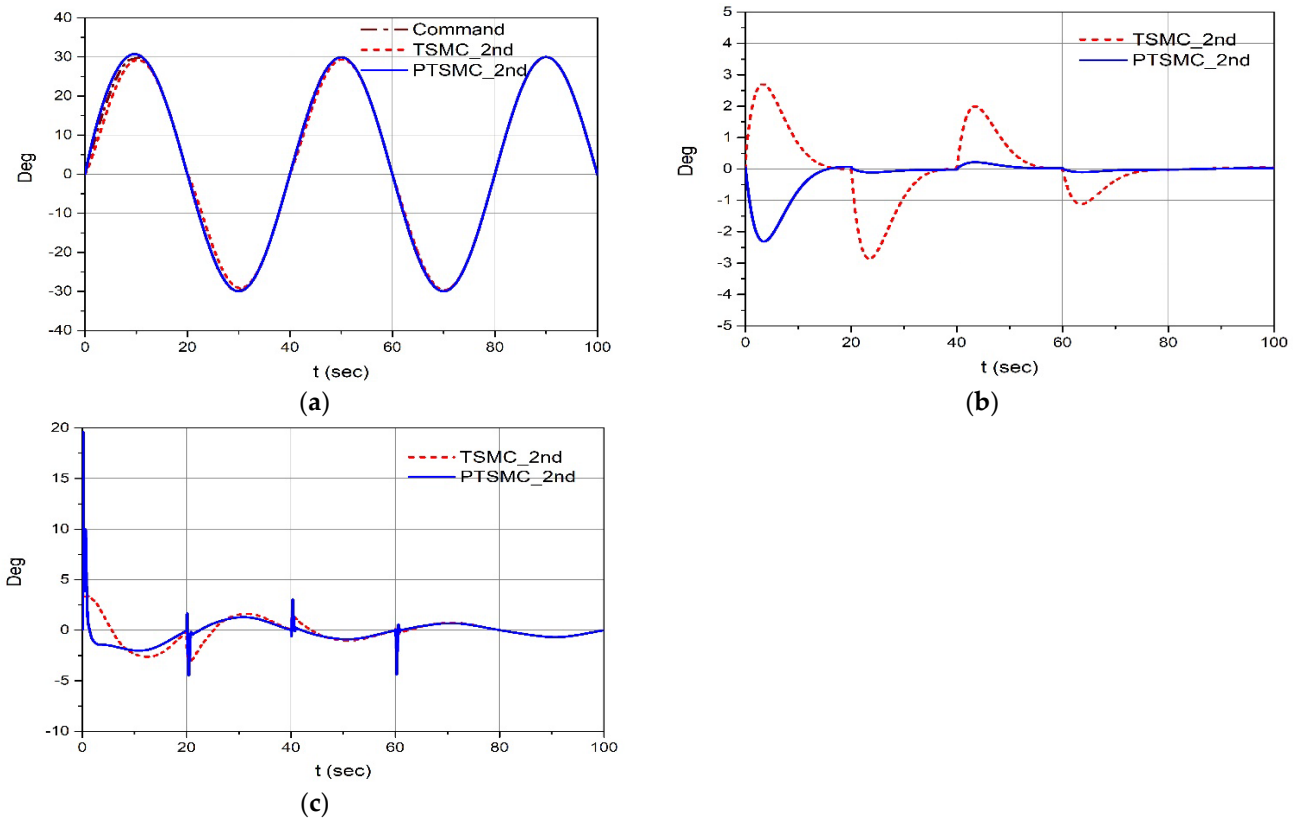


Figure 9. Time response and control input for sine heading-angle command of TSMC_2nd and PTSMC_2nd systems: (a) sine angle output; (b) sine angle error; (c) rudder angle control input.

4.3. Simulation Results for the Multi-Step Command of Surge Velocity and Sine Wave Heading Angle for Pitching-Moment Disturbance

The third simulation was executed to evaluate the control performance under the multi-step command inputs comprising a surge velocity and a heading angle of $30^\circ \sin \omega t$ with $\omega = 0.157 \text{ rad/s}$ for the pitching-moment disturbance input. Figure 10 shows the tracking results of the PTSMC_2nd and P&PTSMC_2nd in the surge channel, where the surge speed command increased gradually until 60 s. After 60 s, the surge speed of 25 knots was maintained until 300 s. In this case, the tracking performances remained almost unchanged despite the pitching-moment disturbance.

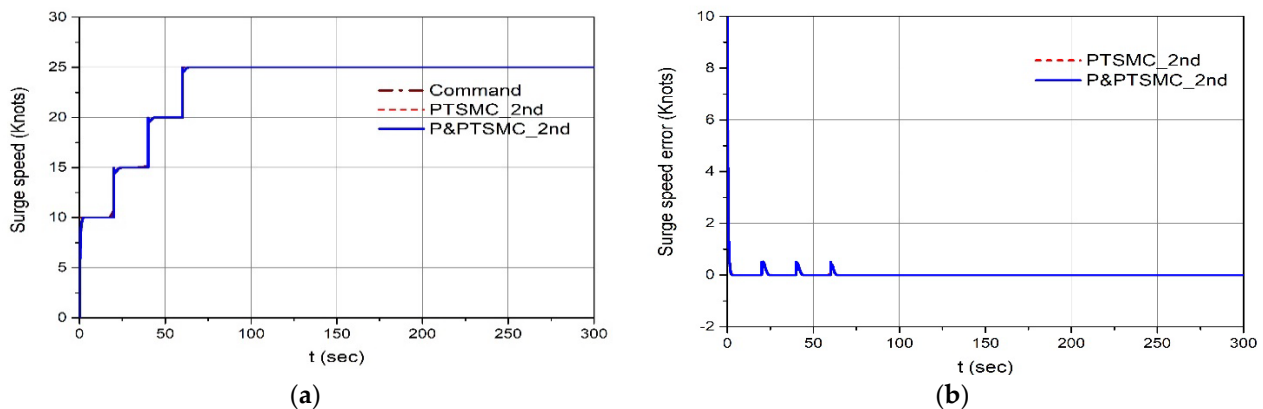


Figure 10. Disturbance response for multi-step surge velocity command of PTSMC_2nd and P&PTSMC_2nd systems: (a) multi-step velocity output; (b) multi-step velocity error.

The pitching moment was generated using (13), (65), and (66) and the result is shown in Figure 11a. The P&PTSMC system was applied to evaluate the disturbance rejection performance using the prescribed-performance control action, in addition to the predefined-time control action without utilizing a disturbance observer. For the generated pitching-moment disturbance input, the heading-angle responses of TSMC_2nd, PTSMC_2nd, and P&PTSMC_2nd are shown in Figure 11b, where TSMC_2nd reveals unstable heading motion because additional control against the disturbance was not provided in TSMC_2nd. Figure 11c shows the tracking errors of each system, where the tracking performances of PTSMC_2nd and P&PTSMC_2nd were better than that of TSMC_2nd. This shows that unstable heading motion oscillations can be generated due to pitching moment when the surge speed reaches a high range.

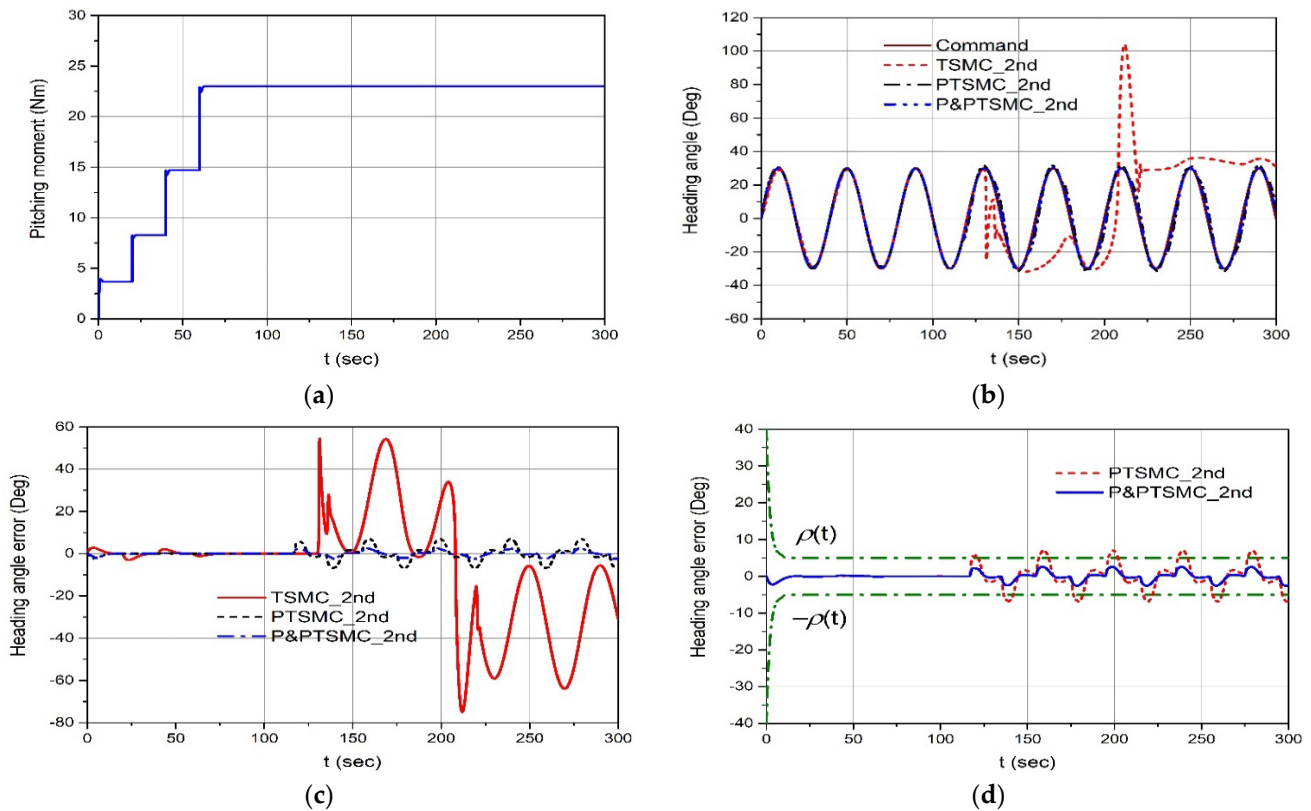


Figure 11. Disturbance response for sine heading-angle command: (a) generated pitching moment; (b) sine heading-angle output; (c) sine heading-angle error of TSMC_2nd, PTSMC_2nd, and P&PTSMC_2nd systems; (d) sine heading-angle error of PTSMC_2nd and P&PTSMC_2nd systems for the prescribed error bound.

However, P&PTSMC_2nd outperformed PTSMC_2nd owing to the application of the prescribed-performance control for enhancing the disturbance rejection performance. As shown in Figure 11d, the tracking error of P&PTSMC_2nd was bounded in the range of $\pm 5^\circ$, though oscillated tracking errors were generated, whereas the tracking error of PTSMC_2nd extended beyond this bound. Therefore, it was seen that only predefined-time control cannot compensate for the disturbance effectively. The values of integral time absolute error (ITAE) and the maximum error of P&PTSMC_2nd decreased by 78% and 37%, respectively, as compared with those of PTSMC_2nd, as shown in Table 5.

Table 5. ITAE and maximum absolute error values of PTSMC_2nd and P&PTSMC_2nd systems.

System	PSMC_2nd	P&PTSMC_2nd
ITAE (sec-deg)	4557 (100%)	3574 (78%)
Maximum absolute error (deg)	7.02 (100%)	2.58 (37%)

In this section, consecutive simulations were conducted to investigate the control performances for the issues of input actuator delay and pitching-moment disturbance with four control systems such as the TSMC_1st, TSMC_2nd, PTSMC_2nd, and P&PTSMC_2nd systems. The simulation results showed that the proposed P&PTSMC_2nd system has outstanding control performance compared to other conventional control systems.

5. Conclusions

In this study, a second-order TSMC system combined with a disturbance rejector based on the concepts of predefined-time control and prescribed-performance control was examined to realize the robust tracking control of a UPH system under control input delay and pitching disturbance due to unstable trim and maneuvering environments. A second-order TSMC system was utilized to accommodate the heading actuator delay caused by delayed hydraulic system response to achieve a stable response in the heading-angle tracking system. Next, predefined-time and prescribed-performance control schemes were considered simultaneously to reject the unmatched pitching-moment uncertainties of the UPH system without explicitly depending on a disturbance observer. Thus, a robust controller equipped with a hybrid disturbance rejector was designed to achieve an excellent response from a UPH control system as compared with the response yielded by the conventional control scheme in conditions with unknown disturbances. Sequential comparative simulations of the UPH model system in cases with input delays and variations in pitching disturbance were executed, and the simulation results demonstrated the efficiency of the proposed control system. Analyzing the simulation results in detail, the TSMC_2nd system could overcome the performance degradation of the TSMC_1st system due to the input delay effect in the heading axis. The PTSMC_2nd system showed a faster response for the selected tracking commands and obtained partial robustness against the disturbance, unlike the conventional TSMC_2nd system. Finally, the P&PTSMC_2nd system showed more improved robust performance of about 20~60% than those of the PTSMC system against the disturbance than that of the PTSMC_2nd system under the same response time.

In a future study, the experimental verification for this work will be executed in an indoor water tank and will be applied to a full-sized UPH on the sea surface.

Funding: This research was funded by the National Research Foundation of Korea (NRF) funded by the Korea government (MSIT) (NRF-2022R1A2C1003137) and the Dongguk University Research Fund of 2021.

Data Availability Statement: Data is contained within the article.

Acknowledgments: The authors thank the support from the Basic Science Research Program through the National Research Foundation of Korea (NRF) funded by the Korea government (MSIT)(NRF-2022R1A2C1003137) and was supported by the Dongguk University Research Fund of 2021.

Conflicts of Interest: The author declares no conflict of interest.

References

1. Savitsky, D. Hydrodynamic design of planning hulls. *Mar. Technol. SNAME News* **1964**, *1*, 71–95. [[CrossRef](#)]
2. Utkin, V.I. Sliding mode control design principles and applications to electric devices. *IEEE Trans. Ind. Electron.* **1993**, *40*, 23–36. [[CrossRef](#)]
3. Chen, X.; Liu, Z.; Zhang, J.; Zhou, D.; Dong, J. Adaptive sliding mode path following control system of the underactuated USV under the influence of ocean currents. *J. Syst. Eng. Electron.* **2018**, *29*, 1271–1283.
4. Qiu, B.; Wang, G.; Fan, Y.; Mu, D.; Sun, X. Adaptive sliding mode trajectory control for unmanned surface vehicle with modeling uncertainties and input saturation. *Appl. Sci.* **2019**, *9*, 1240. [[CrossRef](#)]

5. Kim, H.W.; Lee, J. Robust sliding mode control for a USV water-jet system. *Int. J. Nav. Archit. Ocean Eng.* **2019**, *11*, 851–857. [[CrossRef](#)]
6. Liu, W.; Ye, H.; Yang, X. Model-free adaptive sliding mode control method for unmanned surface vehicle course control. *J. Mar. Sci. Eng.* **2023**, *11*, 1904. [[CrossRef](#)]
7. Khan, M.F.; Islam, R.U.; Iqbal, J. Control strategies for robotic manipulator. In Proceedings of the 2012 International Conference of Robotics and Artificial Intelligence, Rawalpindi, Pakistan, 22–23 October 2012. [[CrossRef](#)]
8. Yu, S.; Yu, X.; Shrinzadeh, B.; Man, Z. Continuous finite-time control for robotic manipulators with terminal sliding mode. *Automatica* **2005**, *41*, 1957–1964. [[CrossRef](#)]
9. Zhao, D.; Li, S.; Gao, F. A new terminal sliding mode control for robotic manipulator. *Int. J. Control* **2009**, *82*, 1804–1813. [[CrossRef](#)]
10. Ahmad, S.; Uppal, A.A.; Azam, M.R.; Iqbal, J. Chattering free sliding mode control and state dependent Kalman filter design for underground gasification energy conversion process. *Electronics* **2023**, *12*, 876. [[CrossRef](#)]
11. Wan, L.; Su, Y.; Shi, B. Global fast terminal sliding mode control based on radial basis function neural network for course keeping of unmanned surface vehicle. *Int. J. Adv. Robot. Syst.* **2019**, *24*, 1729881419829961. [[CrossRef](#)]
12. Fan, Y.; Liu, B.; Wang, G.; Mu, D. Adaptive fast non-singular terminal sliding mode path following control for an underactuated unmanned surface vehicle with uncertainties and unknown disturbances. *Sensors* **2021**, *21*, 7454. [[CrossRef](#)]
13. Alejando, F.G.; Herman, C. Adaptive integral terminal sliding mode control for an unmanned surface vehicle against external disturbances. *IFAC-PapersOnLine* **2021**, *54*, 202–207.
14. Xu, D.; Liu, Z.; Song, J.; Zhou, X. Finite time trajectory tracking with full-state feedback of underactuated unmanned surface vessel based on nonsingular fast terminal sliding mode. *J. Mar. Sci. Eng.* **2022**, *10*, 1845. [[CrossRef](#)]
15. Wang, D.; Kong, M.; Zhang, G.; Liang, X. Adaptive second-order fast terminal sliding-mode formation control for unmanned surface vehicles. *J. Mar. Sci. Eng.* **2022**, *10*, 1782. [[CrossRef](#)]
16. Gong, X.W.; Yi, D.; Tezdogan, T.; Incecik, A. Adaptive neural network and extended state observer-based non-singular terminal sliding mode tracking control for an underactuated USV with unknown uncertainties. *Appl. Ocean Res.* **2023**, *135*, 103560.
17. Ghadimi, P.; Loni, A.; Nowruzi, H.; Dashtimanesh, A.; Tavakoli, S. Parametric study of the effects of trim tabs on running trim and resistance of planning hulls. *Adv. Shipp. Ocean Eng.* **2014**, *3*, 1–12.
18. Mansoori, M.; Fernades, A.C.; Ghassemi, H. Interceptor design of optimum trim control and minimum resistance of plaining boats. *Appl. Ocean Res.* **2017**, *69*, 100–115. [[CrossRef](#)]
19. Sakaki, A.; Ghassemi, H.; Keyvani, S. Evaluation of the hydraulic performance of plaining boat with trim tab and interceptor and its optimization using generic algorithm. *J. Mar. Sci. Appl.* **2018**, *18*, 131–141. [[CrossRef](#)]
20. Chen, Z.; Zhang, Y.; Zhang, Y.; Nie, Y.; Tang, J.; Zhu, S. Disturbance-observer-based sliding mode control design for nonlinear unmanned surface vessel with uncertainties. *IEEE Access* **2019**, *2019*, 148522–148530. [[CrossRef](#)]
21. Xu, D.; Liu, Z.; Zhou, X.; Yang, L.; Huang, L. Trajectory tracking of underactuated unmanned surface vessels: Nonsingular terminal sliding mode control with nonlinear disturbance observer. *Appl. Sci.* **2022**, *12*, 3004. [[CrossRef](#)]
22. Yao, Q. Fixed-time trajectory tracking control for unmanned surface vessels in the presence of model uncertainties and external disturbances. *Int. J. Control* **2022**, *95*, 1133–1143. [[CrossRef](#)]
23. Zhang, J.; Yu, S.; Yan, Y. Fixed-time extended observer-based trajectory tracking and point stabilization control for marine surface vessels with uncertainties and disturbances. *Ocean Eng.* **2019**, *186*, 106109. [[CrossRef](#)]
24. Li, M.; Guo, C.; Yu, H. Filtered extended state observer based line-of-sight guidance for path following of unmanned surface vehicles with unknown dynamics and disturbances. *IEEE Access* **2019**, *7*, 178401–178412. [[CrossRef](#)]
25. Wang, N.; Zhu, X.; Qin, H.; Deng, Z.; Sun, Y. Finite-time extended state observer-based exact tracking control of an unmanned surface vehicle. *Int. J. Robust Nonlinear Control* **2021**, *312*, 1704–1719. [[CrossRef](#)]
26. Fan, Y.; Qiu, B.; Liu, L.; Yang, Y. Global fixed-time trajectory tracking control of underactuated USV based on fixed-time extended state observer. *ISA Trans.* **2023**, *132*, 267–277. [[CrossRef](#)]
27. Sanchez-Torres, J.D.; Sanchez, E.; Loukianov, A.G. Predefined-time stability of dynamical systems with sliding modes. In Proceedings of the 2015 American Control Conference (ACC), Chicago, IL, USA, 1–3 July 2015; pp. 5842–5846.
28. Jimenez-Rodriguez, E.; Sanchez-Torres, J.D.; Loukianov, A.G. On optimal predefined-time stabilization. *Int. J. Robust Nonlinear Control* **2017**, *27*, 3620–3642. [[CrossRef](#)]
29. Sanchez-Torres, J.D.; Gomez-Gutierrez, D.; Lopez, E.; Loukianov, A.G. A class of predefined-time stable dynamical systems. *IMA J. Math. Control Inf.* **2018**, *35*, 1–29. [[CrossRef](#)]
30. Ye, D.; Zou, A.M.; Sun, Z. Predefined-time predefined-bounded attitude tracking control for rigid spacecraft. *IEEE Trans. Aerosp. Electron. Syst.* **2022**, *58*, 464–472. [[CrossRef](#)]
31. Wang, F.; Miao, Y.; Li, C.; Hwang, I. Attitude control of rigid spacecraft with predefined-time stability. *J. Frankl. Inst.* **2020**, *357*, 4212–4221. [[CrossRef](#)]
32. Xie, S.; Chen, Q. Adaptive nonsingular predefined-time control for attitude stabilization of rigid spacecrafts. *IEEE Trans. Circuits Syst. II Express Briefs* **2022**, *69*, 189–193. [[CrossRef](#)]
33. Sanchez-Torres, J.D.; Defoort, M.; Munoz-Vazquez, M. Predefined-time stabilization of a class of nonholonomic systems. *Int. J. Control* **2020**, *93*, 2941–2948. [[CrossRef](#)]
34. Pan, J.; Xiao, T.; Yan, H. Task-space multiple-bipartite consensus for networked heterogenous Euler-Lagrange systems via hierarchical predefined-time control algorithm. *Nonlinear Dyn.* **2023**, *111*, 17095–17108. [[CrossRef](#)]

35. Li, K.; Hua, C.; You, X.; Ahn, K. Output feedback predefined-time bipartite consensus control for high-order nonlinear multiagent systems. *IEEE Trans. Circuits Syst. I Regul. Pap.* **2021**, *68*, 3069–3078. [[CrossRef](#)]
36. Mao, B.; Wu, X.; Lu, J.; Chen, G. Predefined-time bounded consensus of multiagent systems with unknown nonlinearity via distributed adaptive fuzzy control. *IEEE Trans. Cybern.* **2022**, *53*, 2622–2635. [[CrossRef](#)] [[PubMed](#)]
37. Liang, C.D.; Ge, M.F.; Liu, Z.W.; Ling, G.; Liu, F. Predefined-time formation tracking control of networked marine surface vehicles. *Control Eng. Pract.* **2021**, *107*, 104682. [[CrossRef](#)]
38. Jiang, T.; Yan, Y.; Yu, S.H. Adaptive sliding mode control for unmanned surface vehicles with predefined-time tracking performances. *J. Mar. Sci. Eng.* **2023**, *11*, 1244. [[CrossRef](#)]
39. Benchioulis, C.P.; Rovithakis, G.A. Robust adaptive control of feedback linearizable MIMO nonlinear systems with prescribed performance. *IEEE Trans. Autom. Control* **2008**, *53*, 2090–2099. [[CrossRef](#)]
40. Li, Y.; Shao, X.; Tong, S. Adaptive fuzzy prescribed performance control of nontriangular structure nonlinear systems. *IEEE Trans. Fuzzy Syst.* **2020**, *28*, 2416–2426. [[CrossRef](#)]
41. Li, K.; Li, Y. Fuzzy adaptive optimization prescribed performance control for nonlinear vehicle platoon. *IEEE Trans. Fuzzy Syst.* **2023**. [[CrossRef](#)]
42. Han, S.I. Fuzzy supertwisting dynamic surface control for MIMO strict-feedback nonlinear dynamic systems with supertwisting nonlinear disturbance observer and a new partial tracking error constraint. *IEEE Trans. Fuzzy Syst.* **2019**, *27*, 2101–2114. [[CrossRef](#)]
43. Li, S.; Ma, T.; Luo, X.; Yang, Z. Adaptive fuzzy output regulation for unmanned surface vehicles with prescribed performance. *Int. J. Control Autom. Syst.* **2020**, *18*, 405–414. [[CrossRef](#)]
44. Jiang, K.; Mao, L.; Su, Y.; Zheng, Y. Trajectory tracking control for underactuated USV with prescribed performance and input saturation. *Symmetry* **2021**, *13*, 2208. [[CrossRef](#)]
45. Shen, Z.; Wang, Q.; Dong, S.; Yu, H. Prescribed performance dynamic surface control for trajectory-tracking of unmanned surface vessel with input saturation. *Appl. Ocean Res.* **2021**, *113*, 102736. [[CrossRef](#)]
46. Li, J.; Xiang, X.; Dong, D.; Yang, S. Saturated-command-deviation based finite-time adaptive control for dynamic positioning of USV with prescribed performance. *Ocean Eng.* **2022**, *266*, 112941. [[CrossRef](#)]
47. Qu, Y.; Zhao, W.; Yu, Z.; Xiao, B. Distributed prescribed performance containment control for unmanned surface vehicles based on disturbance observer. *ISA Trans.* **2022**, *125*, 699–706. [[CrossRef](#)] [[PubMed](#)]
48. Available online: <https://www.simerics.com/simulation-gallery/planing-hull> (accessed on 27 October 2023).
49. Bhat, S.P.; Bernstein, D.S. Finite-time stability of homogenous systems. In Proceedings of the 1997 American Control Conference, Albuquerque, NM, USA, 6 June 1997; pp. 1073–1078.

Disclaimer/Publisher’s Note: The statements, opinions and data contained in all publications are solely those of the individual author(s) and contributor(s) and not of MDPI and/or the editor(s). MDPI and/or the editor(s) disclaim responsibility for any injury to people or property resulting from any ideas, methods, instructions or products referred to in the content.